ISSN 0021-3640, JETP Letters, 2015, Vol. 102, No. 8, pp. 552–556. © Pleiades Publishing, Inc., 2015.
Original Russian Text © A.M. Tikhonov, 2015, published in Pis'ma v Zhurnal Eksperimental'noi i Teoreticheskoi Fiziki, 2015, Vol. 102, No. 8, pp. 620–625.

CONDENSED MATTER

Solid–Liquid Phase Transition in a Gibbs Monolayer of Melissic Acid at the *n*-Hexane–Water Interface

A. M. Tikhonov

Kapitza Institute for Physical Problems, Russian Academy of Sciences, ul. Kosygina 2, Moscow, 119334 Russia
e-mail: tikhonov@kapitza.ras.ru

Received August 31, 2015

A sharp phase transition from a crystalline state with the area per molecule $A = (17 \pm 1)$ Å^2 to a liquid state with $A = (23 \pm 1)$ Å^2 at the *n*-hexane–water interface in a Gibbs monolayer of melissic acid has been revealed in data of X-ray reflectometry with the use of synchrotron radiation.

DOI: 10.1134/S0021364015200163

The solid–liquid phase transition on the surface of a high-molecular alkane is observed above the bulk melting temperature [1, 2]. The possibility of such a phase transition at an alkane–water interface has been discussed for a long time [3–7]. The observation of a solid–liquid phase transition at the *n*-hexane–water interface in the Gibbs monolayer of a surfactant is reported in this work.

Melissic acid (C_{30}-acid) is not solved in water and is weakly solved in *n*-hexane (C_6H_{14}, density ≈ 0.65 g/cm^3 at 298 K, boiling temperature $T_b \approx 342$ K), which is hardly solved in water under normal conditions. At quite low temperatures, $C_{30}H_{60}O_2$ molecules of acid are adsorbed from a solution in a hydrocarbon solvent on the *n*-hexane–water interface in the form of a solid monolayer (Gibbs monolayer) with the thermodynamic parameters (p, T, c), significantly reducing its energy [8]. According to our new data, with an increase in the temperature T (at the pressure p = 1 atm), a phase transition occurs in the monolayer at a temperature T_c that is determined by the concentration c of the C_{30}-acid in the volume of the solvent serving as a reservoir for the surfactant molecules.

A sample of a macroscopically flat *n*-hexane–water interface oriented by the gravitational force was studied in a stainless-steel cell (see Fig. 1). The dimensions of the interface were 75 × 150 mm [9]. The surface tension of the interface $\gamma(T)$ was measured by the Wilhelmy-plate method with the cell placed in a homemade single-step thermostat [10]. To this end, through holes with a diameter of ~ 1 mm were made in its upper cap and in the cap of the hatch of the cell. The reflectometry of the *n*-hexane–water interface was performed in the hermetically closed cell and its temperature T was controlled in a homemade two-step thermostat. For the entrance and exit of X rays, as well as for the convenient visual observation of the interface, the windows of the cell were fabricated from transparent polyester (Mylar).

A solution of sulfuric acid (pH = 2) in deionized water (Barnstead, NanoPureUV) with a volume of about 100 mL was used as the lower bulk phase. The solution of melissic acid in *n*-hexane with a volume of about 100 mL and the volume concentration $c \approx 0.2$ mmol/kg ($\approx 2 \times 10^{-5}$) was used as the upper bulk phase. C_{30}-acid and *n*-hexane were purchased from the Sigma-Aldrich Corporation. The alkane was preliminarily purified by multiple filtration in a chromatography column through a thick (~30 cm) layer of a fine-grained aluminum oxide powder with a particle diameter of ~0.1 mm. C_{30} acid was doubly purified by recrystallization at room temperature from a supersaturated solution in *n*-hexane, which was prepared by the solution of the acid in *n*-hexane at a temperature of $T \approx 333$ K [11]. Before the measurements of the reflection coefficient R from the interface, the sample was "annealed": the liquids in the cell were heated to $T \cong T_b$ and were then cooled below T_c. Thus, the formation of gas bubbles at the *n*-hexane–water interface at a change in T was prevented in subsequent experiments.

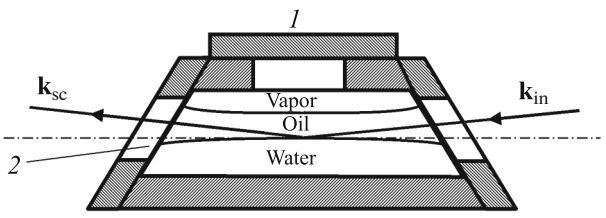

Fig. 1. Airtight sample cell for study of the flat liquid–liquid interface: (*1*) the removable cap of the hatch and (*2*) the transparent polyester (Mylar) window.

A Wilhelmy plate made of a chromatographic paper (Wattman) with a length of $L \approx 10$ mm and a width of ≈5 mm was used in the measurements of $\gamma(T)$. It was fastened to a thin (diameter ~0.25 mm) platinum wire passing through holes in the caps of the thermostat and hatch of the cell (see Fig. 1). The maximum change in the weight of the plate ΔF was fixed by an electric balance (NIMA PS-2) at its slow pulling from the lower phase. Figure 2 shows the dependence $\gamma(T) \approx \Delta F/2L$, which exhibits a feature (kink) at the phase transition temperature $T \approx 291$ K. A change in the slope of $\gamma(T)$ is related to a change in the surface enthalpy $\Delta H = -T_c\Delta(\partial\gamma/\partial T)_{p,c} = (1.1 \pm 0.1)$ J/m^2.

Methods based on the scattering of synchrotron X-ray radiation currently provide the main information on the microscopic structure of (nonpolar organic solvent–water) interfaces, which cannot be obtained from the measurements of such characteristics as the surface tension, capacity of the interface, and surface potential [10, 12]. Unfortunately, relatively strong scattering in the bulk of the hydrocarbon solvent at $\lambda \sim 1$ Å prevents the application of the grazing diffraction method to study the in-plane crystal order at the liquid–liquid interface. The transverse structure of the interface was studied by X-ray reflectometry with the use of synchrotron radiation at the X19C station of the NSLS synchrotron, which was equipped with a universal spectrometer for studying the surface of the liquid [13]. A bending magnet with a critical energy of ~6 keV was a source of radiation for the X19C station. In experiments, a focused monochromatic beam with an intensity of ≈10^{11} photons/s and a photon energy of $E = 15$ keV ($\lambda = (0.825 \pm 0.002)$ Å) was used.

Since the *n*-hexane–water interface is oriented by the gravitational force, the scattering kinematics is conveniently described in the right-handed Cartesian coordinate system whose origin *O* is at the center of the illuminated region, the (*xy*) plane coincides with the interface between the monolayer and water, the *Ox* axis is perpendicular to the beam direction, and the *Oz* axis is normal to the surface and is opposite to the gravitational force (see the inset in Fig. 2). Let $\mathbf{k}_{in}$ and $\mathbf{k}_{sc}$ be the wave vectors of the incident and scattered beams in the direction of the observation point, respectively. In the case of mirror reflection, $\alpha = \beta$ and $\varphi = 0$, where α is the grazing angle in the (*yz*) plane, β is the angle between the scattering direction and the interface in the vertical plane, and φ is the angle between the incident and scattered beams in the (*xy*) plane. The scattering vector $\mathbf{q} = \mathbf{k}_{in} - \mathbf{k}_{sc}$ at mirror reflection has only one nonzero component $q_z = (4\pi/\lambda)\sin(\alpha)$.

The dependence of the reflection coefficient *R* on q_z contains information on the electron density distribution $\rho(z)$ across the *n*-hexane–water interface averaged over a macroscopic area of the illumination region (~100 mm^2). The measurements of *R* at low q_z values are restricted by the transverse dimension and natural divergence (~10^{-4} rad) of a synchrotron radiation beam incident on the sample. The distance between the center of the cell and the nearest slits limiting the vertical dimension of the incident beam is ~120 mm. At the smallest grazing angles of ~6×10^{-4} rad ($q_z \approx 0.01$ Å^{-1}), the vertical dimension of the beam should be ≈15 μm for the illumination region to not exceed the flat segment of the interface (~20 mm). This can be achieved only by suppressing the natural divergence of the beam to ~10^{-5} rad, e.g., by means of two entrance slits with a dimension of ~10 μm at a distance of ~600 mm. At large grazing angles ($q_z > 0.2$ Å^{-1}), the maximum vertical dimension of the entrance slits, 0.4 mm, is limited by the chosen vertical angular resolution of the detector, $2\Delta\beta \approx 10^{-3}$ rad (a slit with a vertical dimension of 0.8 mm at a distance of ≈ 680 mm from the center of the sample). The measurements were performed with the resolution $\Delta\varphi \approx 10^{-2}$ rad of the detector in the horizontal plane.

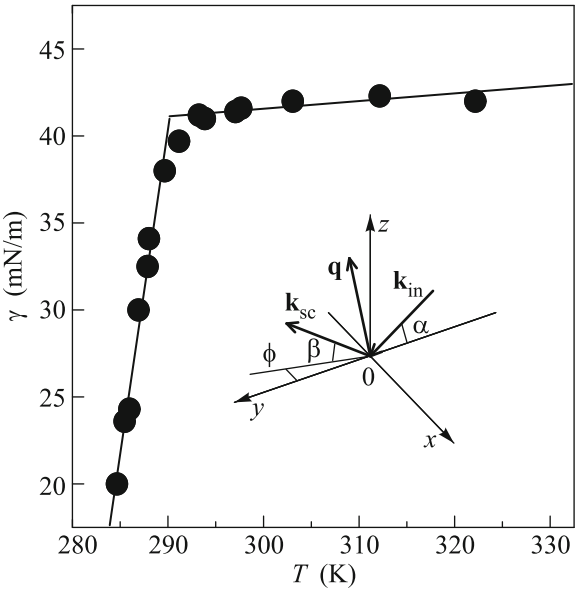

Fig. 2. Temperature dependence of the surface tension of the *n*-hexane–water interface at the concentration $c \approx 0.2$ mmol/kg of C_{30}-acid in *n*-hexane. The bending point corresponds to $T_c \approx 291$ K. The inset shows the kinematics of scatter at the *n*-hexane–water interface. The (*xy*) plane coincides with the interface; the *Ox* axis is perpendicular to the beam direction; the *Oz* axis is normal to the surface and is opposite to the gravitational force; $\mathbf{k}_{in}$ and $\mathbf{k}_{sc}$ are the wave vectors of the incident and scattered beams in the direction of the observation point, respectively; $\mathbf{q} = \mathbf{k}_{in} - \mathbf{k}_{sc}$ is the scattering vector; and α and β are the grazing and scattering vectors in the plane normal to the surface, respectively.

Figures 3 and 4 show the dependences $R(q_z)$ for the *n*-hexane–water interface at various temperatures above and below the phase transition, respectively. At $q_z < (4\pi/\lambda)\alpha_c \approx 0.01$ Å^{-1}, the incident beam undergoes

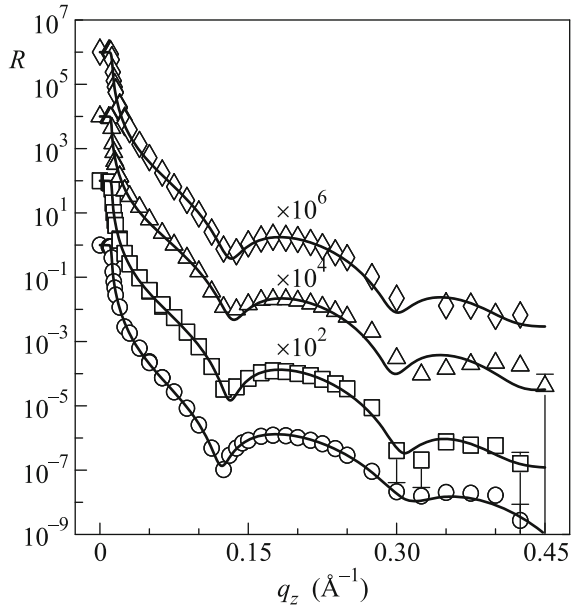

Fig. 3. Reflection coefficient R versus q_z for the n-hexane–water interface at (diamonds) 293.4, (triangles) 290.1, (squares) 289.2, and (circles) 288.3 K. The solid lines correspond to the two-layer model of the absorbed layer.

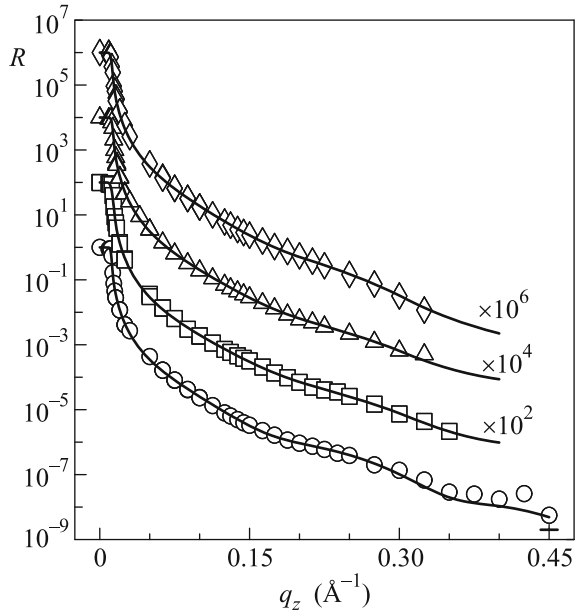

Fig. 4. Reflection coefficient R versus q_z for the n-hexane–water interface at (diamonds) 334.2, (triangles) 317.9, (squares) 308.1, and (circles) 298.2 K. The solid lines correspond to the two-layer model of the absorbed layer described in the main text.

the total external reflection $R \approx 1$. The critical angle α_c is determined by the difference $\Delta\rho \approx 0.11$ $e^-/\text{Å}^3$ between the volume electron densities of n-hexane and water: $\alpha_c = \lambda\sqrt{r_e\Delta\rho/\pi} \approx 10^{-3}$ rad, where $r_e = 2.814 \times 10^{-5}$ Å is the classical radius of the electron. The data presented in Figs. 3 and 4 clearly demonstrate that the reflection curve changes sharply near T_c. In addition to the dependences $R(q_z)$, we measured the temperature dependence of the reflection coefficient near T_c at a fixed value of $q_z = 0.05$ Å^{-1} (see Fig. 5) with the same spatial resolution of the detector.

The analysis of Figs. 3 and 4 shows that $C_{30}H_{60}O_2$ molecules are absorbed in the form of a monolayer on the n-hexane–water interface. In order to obtain detailed information on the structure of the interface from $R(q_z)$, we used the simplest qualitative two-layer model (slab model) of an adsorbed layer with five fitting parameters in which the density profile $\rho(z)$ is based on the error function [14]. The lower limit of the standard deviations σ_j of the positions of the jth interfaces of the bilayer ($j = 0, 1, 2$) from the reference value z_j is determined by the capillary width $\sigma_{cw}^2 = (k_BT/2\pi\gamma)\ln(Q_{max}/Q_{min})$ (k_B is the Boltzmann constant), which is specified by the short-wavelength limit in the spectrum of capillary waves $Q_{max} = 2\pi/a$ (where $a \approx 10$ Å is the order of magnitude of the molecular radius) and $Q_{min} = q_z^{max}\Delta\beta$ (where $q_z^{max} \approx 0.45$ Å^{-1}) [15–17]. Under the assumption that $\sigma_j = \sigma_0$ for all j values, the structure factor of the surface in the first Born approximation has the form [18]

$$\frac{R(q_z)}{R_F(q_z)} \approx \left|\frac{1}{\Delta\rho}\sum_{j=0}^{2}(\rho_{j+1} - \rho_j)e^{-iq_zz_j}\right|^2 e^{-\sigma_0^2q_z^2}, \qquad (1)$$

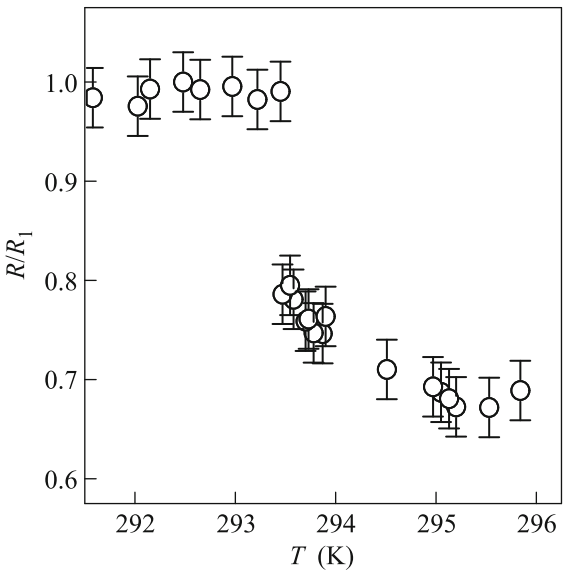

Fig. 5. Temperature dependence of the normalized reflection coefficient R/R_1 at $q_z = 0.05$ Å^{-1}, where R_1 is the reflection coefficient at $T \approx 292.2$ K.

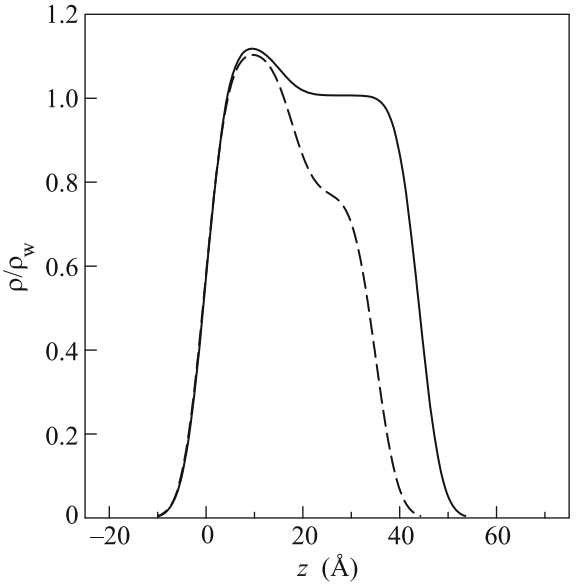

Fig. 6. Model electron density profiles for a monolayer of melissic acid normalized to the electron density in water under normal conditions ($\rho_w = 0.333\ e^-/Å^3$) obtained within the two-layer model of (solid line) the low-temperature phase of the monolayer (T = 293.4 K) and (dashed line) the high-temperature phase of the monolayer (T = 317.9 K).

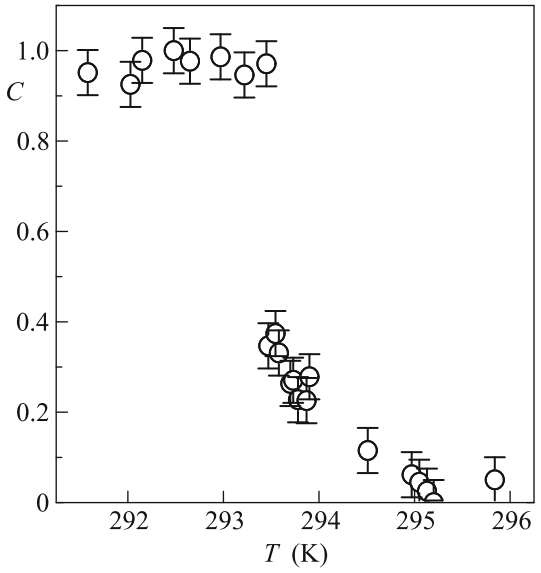

Fig. 7. Temperature dependence of the coverage of the surface by domains of the low-temperature phase C. The points are obtained from the data presented in Fig. 5 with the use of Eq. (2), where R_1 and R_2 are the reflection coefficients at $T \approx 292$ and 295 K, respectively.

where ρ_j is the electron density in the jth layer; ρ_0 and ρ_3 are the electron densities in water and n-hexane, respectively; and $R_F(q_z) \approx [q_z - (q_z^2 - q_c^2)^{1/2}/[q_z + (q_z^2 - q_c^2)^{1/2}]^2$ is the Fresnel function. The calculated reflection curves are shown by solid lines in Figs. 3 and 4. The model profiles $\rho(z)$ for monolayers of (solid line) low- and (dashed line) high-temperature phases are shown in Fig. 6.

The variation of the parameters in the model of the monolayer is in agreement with the molecular structure of melissic acid, which has a hydrophilic head part and a hydrophobic hydrocarbon tail. The first hydrophilic layer of the monolayer for the low-temperature phase, which is in direct contact with water, includes –COOH polar groups and has the density $\rho_1 = (1.16 \pm 0.05)\rho_w$ and the thickness $L_1 = z_1 - z_0 = (15 \pm 2)$ Å ($\rho_w = 0.333\ e^-/Å^3$ is the electron density in water under normal conditions). If the width of this layer is fixed $L_1 < 10$ Å at fitting, the quality of fitting at high q_z values worsens significantly. The second layer with the thickness $L_2 = z_2 - z_1 = (29 \pm 2)$ Å is formed by hydrocarbon chains with the density $\rho_2 = (1.01 \pm 0.02)\rho_w$. The fitting parameter σ_0 varies from 3.6 to 4.5 Å, which coincides within the errors with the calculated σ_{cw} value. The total thickness of the monolayer is (42 ± 3) Å, which also coincides within the errors with the calculated total length (40.8 Å = 29 × 1.27 Å(C–C) + 1.5 Å(CH3) + 2.5 Å(–COOH)) of the $C_{30}H_{60}O_2$ molecule (it contains 256 electrons). Thus, all molecules in this phase of the monolayer are elongated along the normal to the surface and the area per molecule of C_{30} acid is $A = 256/(\rho_1 L_1 + \rho_2 L_2) = (17 \pm 1)$ Å^2. This value corresponds to the densest crystal phase of alkanes [19].

The hydrophilic layer in the high-temperature phase has the density $\rho_1 = (1.12 \pm 0.02)\rho_w$ and thickness $L_1 = (18 \pm 2)$ Å. The electron density in the second layer with the thickness $L_2 = (18 \pm 2)$ Å is $\rho_1 = (0.77 \pm 0.02)\rho_w$. The fitting value $\sigma_0 = (4.0 \pm 0.2)$ Å coincides within the errors with the value $\sigma_{cw} \approx 3.6$ Å calculated with the data for $\gamma(T)$. The value $A = (23 \pm 1)$ Å^2 for the high-temperature phase corresponds to a high-molecular hydrocarbon liquid [19].

The monotonic temperature dependence $R(T)$ at a fixed q_z value (see Fig. 7) indicates incoherent reflection from the intraplane structure of the interface. Since our data show that the relative contribution from diffuse scattering at the interface to the reflected power is small (~10^{-3}), R in the first approximation can be represented in the form of a linear function of the coverage of the surface $C(T)$ by domains of the low-temperature phase of C_{30} acid [20]:

$$R \approx C(T)R_1 + [1 - C(T)]R_2, \qquad (2)$$

where R_1 and R_2 are the R values for low-temperature ($C(T) = 1$) and high-temperature ($C(T) = 0$) phases, respectively. Circles in Fig. 7 represent the calculated dependence for $C(T) \approx (R - R_2)/(R_1 - R_2)$ at $q_z = 0.05$ Å^{-1}. According to this dependence, the phase transition in the monolayer at $T_c \approx 293.5$ K is sharp:

the surface is rearranged in the temperature interval $\leqslant 0.5$ K. A small difference (~2 K) of the T_c value for this sample from the temperature of the bending point $\gamma(T)$ in Fig. 2 is due both to uncertainty in its determination and to a small difference in the volume concentration c between the samples.

The analysis of the experimental results reveals two important features of the critical behavior of the crystalline monolayer of melissic acid at the interface. First, a phase transition associated with melting occurs in this monolayer with an increase in the temperature. Such a behavior differs from the critical behavior of monolayers of high-molecular saturated and fluorocarbon alcohols at this interface, where an increase in the temperature is accompanied by phase transitions of evaporation and sublimation of monolayers, respectively [6]. Second, according our data, the total electron density in the monolayer at T_c decreases stepwise by $\Delta A/A \approx 30\%$. This behavior is significantly different from the critical behavior of monolayers of high-molecular alcohols at the *n*-hexane–water interface, where phase transitions occur in a certain temperature range, as well as from the crystallization of monolayers of CTAB and STAB cationic surfactants, where two critical temperatures were observed [7].

To conclude, the reported data illustrate the solid–liquid phase transition in the Gibbs monolayer at the *n*-hexane–water interface. With an increase in the temperature in a narrow vicinity of T_c, a significant fraction of adsorbed molecules of C_{30} acid leave the interface and are solved in the bulk of *n*-hexane. In this case, the thickness of the monolayer $L_1 + L_2$ decreases by ≈15% and A increases by ≈30%.

I am grateful to Profs. M.L. Schlossman and V.I. Marchenko for stimulating discussions of the experimental results. The work at the NSLS synchrotron was supported by the US Department of Energy (contract no. DE-AC02-98CH10886). The work at the X19C station was supported by the ChemMatCARS Foundation, University of Chicago, University of Illinois at Chicago, and Stony Brook University.

REFERENCES

1. J. C. Earnshaw and C. J. Hughes, Phys. Rev. A **46**, R4494 (1992).
2. X. Z. Wu, E. B. Sirota, S. K. Sinha, B. M. Ocko, and M. Deutsch, Phys. Rev. Lett. **70**, 958 (1993).
3. J. T. Davies and E. K. Rideal, *Interfacial Phenomena* (Academic, New York, 1963).
4. D. M. Mitrinovic, A. M. Tikhonov, M. Li, Z. Huang, and M. L. Schlossman, Phys. Rev. Lett. **85**, 582 (2000).
5. Q. Lei and C. D. Bain, Phys. Rev. Lett. **92**, 176103 (2004).
6. M. L. Schlossman and A. M. Tikhonov, Ann. Rev. Phys. Chem. **59**, 153 (2008).
7. L. Tamam, D. Pontoni, Z. Sapir, Sh. Yefet, E. Sloutskin, B. M. Ocko, H. Reichert, and M. Deutsch, Proc. Nat. Acad. Sci. **108**, 5522 (2011).
8. A. M. Tikhonov, H. Patel, S. Garde, and M. L. Schlossman, J. Phys. Chem. B **110**, 19093 (2006).
9. D. M. Mitrinovic, Z. J. Zhang, S. M. Williams, Z. Q. Huang, and M. L. Schlossman, J. Phys. Chem. B **103**, 1779 (1999).
10. A. W. Adamson, *Physical Chemistry of Surfaces*, 3rd ed. (Wiley, New York, 1976).
11. T. Takiue, A. Yanata, N. Ikeda, K. Motomura, and M. Aratono, J. Phys. Chem. **100**, 13743 (1996).
12. M. L. Schlossman, M. Li, D. M. Mitrinovic, and A. M. Tikhonov, High Perform. Polym. **12**, 551 (2000).
13. M. L. Schlossman, D. Synal, Y. Guan, M. Meron, G. Shea-McCarthy, Z. Huang, A. Acero, S. M. Williams, S. A. Rice, and P. J. Viccaro, Rev. Sci. Instrum. **68**, 4372 (1997).
14. F. P. Buff, R. A. Lovett, and F. H. Stillinger, Phys. Rev. Lett. **15**, 621 (1965).
15. A. M. Tikhonov, J. Phys. Chem. C **111**, 930 (2007).
16. M. P. Gelfand and M. E. Fisher, Physica (Amsterdam) **166A**, 1 (1990).
17. P. S. Pershan and M. L. Schlossman, *Liquid Surfaces and Interfaces: Synchrotron X-ray Methods* (Cambridge Univ. Press, Cambridge, 2012).
18. J. Daillant, L. Bosio, B. Harzallah, and J. J. Benattar, J. Phys. II **1**, 149 (1991).
19. D. M. Small, *The Physical Chemistry of Lipids* (Plenum, New York, 1986).
20. A. M. Tikhonov, S. V. Pingali, and M. L. Schlossman, J. Chem. Phys. **120**, 11822 (2004).

Translated by R. Tyapaev